Available online at www.sciencedirect.com
ScienceDirect
International Journal of Heat and Mass Transfer 50 (2007) 1087–1096
International Journal of HEAT and MASS TRANSFER
www.elsevier.com/locate/ijhmt

An analytical solution for thermally fully developed combined pressure – electroosmotically driven flow in microchannels

Azad Qazi Zade, Mehrdad T. Manzari *, Siamak K. Hannani

Center of Excellence in Energy Conversion, School of Mechanical Engineering, Sharif University of Technology, P.O. Box 11365-3567, Tehran, Iran

Received 19 December 2005; received in revised form 27 June 2006
Available online 27 October 2006

Abstract

An analytical solution is presented to study the heat transfer characteristics of the combined pressure – electroosmotically driven flow in planar microchannels. The physical model includes the Joule heating effect to predict the convective heat transfer coefficient in two dimensional microchannels. The velocity field, which is a function of external electrical field, electroosmotic mobility, fluid viscosity and the pressure gradient, is obtained by solving the hydrodynamically fully-developed laminar Navier–Stokes equations considering the electrokinetic body force for low wall zeta potentials. Then, assuming a thermally fully-developed flow, the temperature distribution and the Nusselt number is obtained for a constant wall heat flux boundary condition. The fully-developed temperature profile and the Nusselt number depend on velocity field, channel height, solid/liquid interface properties and the imposed wall heat flux. A parametric study is presented to evaluate the significance of various parameters and in each case, the maximum heat transfer rate is obtained.

Keywords: Heat transfer; Electrokinetic; Joule heating; Microchannel

1. Introduction

The rise in microelectronic heat fluxes and the non-uniformities in heat dissipation have increased the demand for highly efficient electronic cooling technologies. Because of the push to increase the functionality and to decrease the floor space consumed, there is an ever increasing demand for higher power-density, which in turn requires compact, reliable and efficient heat sinks. Also, it is known that the operation efficiency of an electronic component is highly temperature dependent. In recent years, there has been an extensive research into the design of microfluidics systems for compact cooling technologies. Investigations have been conducted to better understand the fluid flow and heat transfer characteristics in silicon-based microchannel heat sinks designed for applications in electronic cooling. These silicon based microchannel heat sinks combine the attributes of high material compatibility, high surface area per unit volume ratios, and large potential heat transfer performance, with highly sophisticated and economic fabrication processes. Such advantages make these silicon based microchannel heat sinks highly attractive for a wide variety of commercial applications. Also at the microscale, generation of fluid motion is a challenge since the working pressure is substantially high. Although micropumps which are capable of delivering such pressures exist [1], their moving components are complicated to design and fabricate, and they are prone to mechanical failure due to fatigue and fabrication defects which in turn make them unsuitable for microfluidic applications. On the other hand, electroosmotic flow presents a feasible alternative to pressure driven flow in liquid delivery systems, featuring better flow control with no moving parts. Several previous studies have reported successful demonstration of electro-osmotic pumping systems [1–4].

First observed by Reuss [5], electroosmosis is the process of inducing motion to ionized liquid, adjacent to a

* Corresponding author. Tel.: +98 21 6616 5689; fax: +98 21 6600 0021.
E-mail address: mtmanzari@sharif.edu (M.T. Manzari).

0017-9310/$ - see front matter © 2006 Elsevier Ltd. All rights reserved.
doi:10.1016/j.ijheatmasstransfer.2006.07.037

Nomenclature

c_p	fluid specific heat
D	channel height
E_x	external electrical field
g	dimensionless volumetric heat generation
h	convective heat transfer coefficient
i_e	current density
k	thermal conductivity
Nu	Nusselt number
p	pressure
Pe	Peclet number
q''	wall heat flux
q'''	volumetric heat generation
T	temperature
T_m	bulk mean temperature
T_w	wall temperature
u	local fluid velocity
u_{eo}	electroosmotic velocity
U	average velocity
x	streamwise coordinate
y	wall – normal coordinate
Y	dimensionless wall – normal coordinate

Greek symbols

α	thermal diffusivity
ε	fluid dielectric constant
ϕ	charge distribution
Γ	channel height to Debye length ratio
λ_D	Debye length
μ	dynamic viscosity
μ_{eo}	electroosmotic mobility
ρ	fluid density
σ	liquid electrical resistivity
θ	normalized temperature
θ_w	wall normalized temperature
ψ	auxiliary dimensionless function
ζ	wall zeta potential

stationary charged surface, under an applied external electric field. Most solid surfaces acquire a relative electric charge when brought in contact with an aqueous (polar) solution. The charged surface attracts counter-ions and repels co-ions as shown in Fig. 1a. The net effect is the formation of a region close to the charged surface called the electric double layer (EDL) in which there is an excess of counter-ions over co-ions. The charge distribution in the fluid therefore falls from its maximum value near the wall to a zero charge in the core of the flow. This maximum value is characterized by the so-called zeta potential, ς. In a simple model of the charge distribution, the plane separating the inner immobile layer and the outer diffuse layer is called the shear plane. The zeta potential of the double layer is the potential at the shear plane. The thickness of the electrical double layer is on the order of the Debye length, λ_D, of the solution [6]. If an external electrical field is applied parallel to the dielectric wall, Columbic forces are exerted on the mobile ions in the net positive layer above the shear plane and consequently the electro-migration of these ions drives the bulk liquid through viscous interaction, as depicted in Fig. 1b. The resulting velocity profile is dependent upon a number of factors such as electroosmotic properties of solid/liquid combination (electroosmotic mobility), dimensions of the channel, external electric field, pressure gradient, fluid viscosity, etc.

It has been shown that the hydrodynamic characteristics of the combined pressure-electroosmotically driven flow differ from both conventional pressure driven flow and pure electroosmotic flow [7–9]. Therefore, a significantly different thermal behavior may be expected from such systems. The differences are originated from two main sources. Firstly, the velocity profile of the combined pressure-electroosmotically driven flow is quite different from the pressure driven flow or the pure electroosmotic flow. This velocity profile obviously affects the temperature distribution in the channel. Secondly, in the electroosmotic flow, the applied electric field induces an electric current in the fluid which results in the so-called Joule heating effect. The presence of the Joule heating effect, which might be regarded as a distributed volumetric heat generation, would also affect the thermal transport properties of the flow.

The hydrodynamics of a fully-developed pure electroosmotic flow has been analyzed analytically. Several earlier

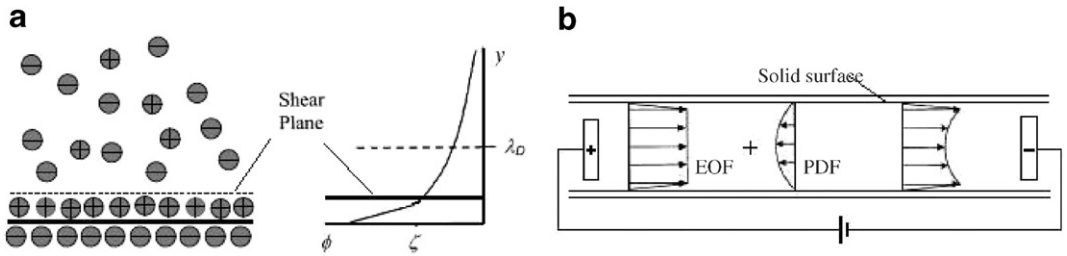

Fig. 1. Schematic structure of electric double layer: (a): Zeta potential and the characteristic length of the double layer λ_D, (b): Flow principal of the EO pumps.

papers discussed the hydrodynamic behavior of pure electroosmotic flow in capillaries [10–12]. More recent work are by Mala et al. [7] on parallel-plate microchannels, and Yang et al. [13] on microchannels with rectangular cross section where they invoked the classic Debye–Huckel approximation to allow for an analytical solution. Recently, several other aspects of the hydrodynamics of electroosmotic flow were studied analytically. Among these are transient behavior of the flow field [8,9,14], electrical conductivity gradient in the streamwise direction [15], developing flow field in the entry region [3,16] and the effect of variable wall zeta potential on the flow field [17,18]. Also, experimental studies on the characteristics of the steady-state electroosmotic flow have been reported [18–24].

A detailed discussion about the thermal behavior of the conventional pressure driven flow can be found in heat transfer textbooks. Also, for the case in which the Debye length is small compared to the channel dimensions and the pressure gradient is negligible, i.e. when the slug flow prevails [3], solutions for laminar thermally developing and fully developed cases exist [25]. The effect of the EDL and the flow-induced electrokinetic field on the flow and heat transfer characteristics in microchannels has been studied in [13,26,27]. It was reported that the flow induced electrokinetic potential increases the resistance on the flow and hence exhibits higher friction factor and moreover, the Nusselt number is lower compared to the conventional pressure driven flow. Only little work can be found in the literature concerning the thermal behavior of the fully developed electroosmotic flow. Maynes and Webb [28,29] presented analytical solutions for thermally fully developed electroosmotic flow in circular and parallel plate microchannels considering the Joule heating effect and viscous dissipation. They also studied the convective heat transfer of thermally (and hydrodynamically) fully developed combined pressure-electroosmotically driven flow in circular microchannels [30]. In this latter work, Maynes and Webb studied the effect of various parameters such as the ratio of Debye length to the tube radius, liquid electrical resistivity and the ratio of the pressure to electroosmotic driving forces on the heat transfer characteristics of the combined pressure-electroosmotically driven flow. They reported that at high channel height to Debye length ratios, the velocity profile is essentially a superposition of the slug flow and the pressure driven flow. Also, their results show that the Nusselt number is strongly dependent on the magnitude of the volumetric heat generation. Their work however was a parametric study considering the effect of one parameter at a time, which is not the case in practical situations when both flow and heat transfer effects are dealt with. Moreover, the maximum attainable heat transfer was not investigated. In reality, as the external electrical field varies, both the velocity profile and volumetric heat generation change. As a consequence, the temperature distribution and heat transfer coefficient change. In fact, all these variations are coupled and occur simultaneously and their mutual relations should be taken into account in the analysis. To the best of authors' knowledge, such a coupling which takes into account all the variations simultaneously has not been investigated yet. This is addressed in the current paper.

This paper presents an analytical solution for a thermally (and hydrodynamically) fully developed combined pressure electroosmotic driven flow between parallel plates for a constant wall heat flux boundary condition. The heat transfer characteristics of the problem are described and maximum heat transfer rate is obtained for a range of design parameters.

2. Mathematical model

2.1. Flow model

Consider the fully developed laminar flow of an incompressible fluid in a 2D microchannel where the driving forces are the pressure difference between the two ends of the channel and the electrokinetic body force. A schematic of the problem is shown in Fig. 2.

In a steady-state and hydrodynamically fully developed flow, the streamwise momentum equation can be written as

$$\mu\frac{\mathrm{d}^2u}{\mathrm{d}y^2}-\frac{\mathrm{d}p}{\mathrm{d}x}=\varepsilon\frac{\mathrm{d}^2\phi}{\mathrm{d}y^2}E_x \tag{1}$$

where μ and ε are the dynamic viscosity and the dielectric constant of the fluid, respectively. Also, ϕ is the charge distribution and E_x is the applied external electric field in the flow direction. In general, the physical properties of the fluid are temperature dependent and therefore the momentum and energy equations are coupled. However, in this work, the physical properties of the fluid are assumed to be constant and therefore the momentum and energy equations are not coupled. For high channel height to Debye length ratios ($\Gamma = D/\lambda_D$), which is assumed to be the case in the present study, the velocity profile due to the electroosmotic effect can be approximated by the classical Helmholtz–Smoluchowski equation [31,32]. In this case, the velocity profile due to the electroosmotic driving force is a slug-like profile and is written as

$$u_{eo}=\frac{\varepsilon\zeta}{\mu}E_x \tag{2}$$

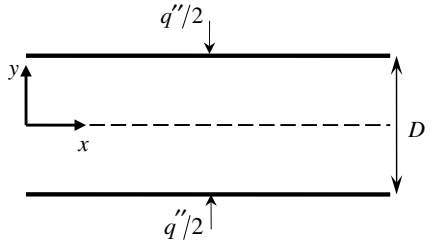

Fig. 2. Problem definition.

where ζ is the wall zeta potential and the term $\varepsilon\zeta/\mu$ is usually referred to as the electroosmotic mobility, μ_{eo}. The above velocity distribution is fairly accurate for $\Gamma \geqslant 100$ [28,31]. Since the magnitude of the Debye length is nominally 10–500 nm, all the channel heights considered here are higher than 50 μm to meet the criterion. Therefore, the velocity distribution for the combined pressure-electroosmotic driven flow is given by

$$u = \mu_{eo}E_x - \frac{D^2}{8\mu}\frac{dp}{dx}(1-4Y^2) \tag{3}$$

where $Y = y/D$ is the dimensionless channel height and the second term on the right hand side of Eq. (3) is due to the pressure gradient and is the classical parabolic distributions similar to the Poiseuille flow.

2.2. Thermal transport

Considering the steady-state hydrodynamically fully-developed flow with constant physical properties in a 2D channel, the energy equation with volumetric heat generation can be expressed as

$$\frac{u}{\alpha}\frac{\partial T}{\partial x} = \frac{\partial^2 T}{\partial x^2} + \frac{\partial^2 T}{\partial y^2} + \frac{q'''}{k} \tag{4}$$

where T is the temperature, k and α are thermal conductivity and diffusivity of the fluid, respectively, and q''' is the volumetric heat generation in the fluid. In general, q''' consists of both the Joule heating and the viscous dissipation terms. For large values of Γ the viscous dissipation term can be neglected compared to the Joule heating effect [29]. Therefore, in the present study, the viscous dissipation is neglected and the volumetric heat generation is only due to Joule heating effect and is equal to $q''' = \sigma i_e^2$ in which i_e is the current density and σ is the liquid electrical resistivity. For low zeta potentials, the current density is essentially uniform across the channel height [6,10]. According to Ohm's law $i_e = E_x/\sigma$, therefore, the uniform volumetric heat generation can be expressed as $q''' = E_x^2/\sigma$. An overall energy balance on the fluid yields

$$\frac{dT_m}{dx} = \frac{1}{D\rho U c_p}(q'' + Dq''') \tag{5}$$

where q'' represents the heat flux rate per unit area and ρ, c_p and U are fluid density, specific heat and average velocity, respectively. Also, the bulk mean temperature T_m is defined as

$$T_m = \frac{1}{U}\int uT\,dY \tag{6}$$

If the flow is thermally fully-developed, the classical dimensionless temperature becomes invariant with x [25]

$$\frac{\partial}{\partial x}\left(\frac{T_w - T}{T_w - T_m}\right) = 0 \tag{7}$$

where T_w is the wall temperature. This yields

$$\frac{\partial T}{\partial x} = \frac{dT_w}{dx} - \frac{T_w - T}{T_w - T_m}\frac{dT_w}{dx} + \frac{T_w - T}{T_w - T_m}\frac{dT_m}{dx} \tag{8}$$

Also, invoking the definition of a thermally fully-developed flow, Eq. (7), the temperature distribution can be written in the following form

$$T = T_w - \frac{q''}{h}\psi(Y) \tag{9}$$

where ψ is a function of Y only and $h = q''/(T_w - T_m)$ is the convective heat transfer coefficient. In order to proceed, the relevant boundary conditions need to be specified. Usually two typical boundary conditions are used in connection with the energy equation; constant wall heat flux and constant wall temperature. However, in order to achieve an analytical solution for the constant wall temperature boundary condition, the axial conduction term, $\partial^2 T/\partial x^2$, in the energy equation is neglected compared to the axial convection term, $(u/\alpha)\partial T/\partial x$. This assumption is true only when the Peclet number, $Pe = (uD)/\alpha$, is far greater than 1. In the problems considered in this article, the velocities are of orders of cm/s and the channels height is of order of 100 μm. This means that the Peclet number is of $O(1)$ and the axial conduction cannot be neglected. Therefore, only the constant wall heat flux boundary condition is considered here.

If the imposed wall heat flux q'' is constant, it can be easily shown that in a thermally fully-developed flow $\partial T/\partial x = dT_m/dx = \text{constant}$ and $\partial^2 T/\partial x^2 = 0$ [25]. Also, using Eq. (9), the energy equation reduces to

$$\frac{d^2\psi}{dY^2} = Nu\left[g - \frac{u(Y)}{U}(1+g)\right] \tag{10}$$

where $g = (q'''D)/q''$ is the dimensionless volumetric heat generation and $Nu = hD/k$ is the Nusselt number. Considering Eq. (9), the boundary conditions can be written as

$$\left.\frac{\partial\psi}{\partial Y}\right|_{Y=0} = 0 \text{ and } \psi|_{Y=-\frac{1}{2}} = 0 \tag{11}$$

Substituting Eq. (3) into Eq. (10) and integrating it twice subjected to boundary conditions (11), yields

$$\psi = Nu\left[A\left(\frac{1}{4} - Y^2\right) + B\left(\frac{1}{16} - Y^4\right)\right] \tag{12}$$

where the parameters A and B are functions of the dimensionless volumetric heat generation and are defined as

$$A = \frac{1+g}{2U}\left(\mu_{eo}E - \frac{D^2}{8\mu}\frac{dp}{dx}\right) - \frac{g}{2} \tag{13a}$$

$$B = \frac{1+g}{U}\frac{D^2}{24\mu}\frac{dp}{dx} \tag{13b}$$

The unknown Nusselt number Nu in Eq. (12) is determined by evaluating the bulk mean temperature, Eq. (6), which results in

$$1 = \frac{1}{U}\int_{-1/2}^{1/2}\psi u(Y)\,dY \tag{14}$$

Therefore the Nusselt number can be expressed as

$$Nu = \frac{U}{I} \tag{15}$$

where

$$I = \int_{-1/2}^{1/2} u(Y)\left[A\left(\frac{1}{4} - Y^2\right) + B\left(\frac{1}{16} - Y^4\right)\right] \mathrm{d}Y \tag{16}$$

This integral can be evaluated analytically to compute the Nusselt number. Substituting the velocity field, Eq. (3), into Eq. (16), results in

$$I = A\left[\frac{\mu_{eo}E}{6} - \frac{D^2}{60\mu}\left(\frac{\mathrm{d}p}{\mathrm{d}x}\right)\right] + B\left[\frac{\mu_{eo}E}{20} - \frac{D^2}{210\mu}\left(\frac{\mathrm{d}p}{\mathrm{d}x}\right)\right] \tag{17}$$

It should be noted that the resulting Nusselt number is a function of the dimensionless volumetric heat generation, g, and as a result it is a function of the external electric field.

3. Results and Discussion

In this section, a parametric study is presented to evaluate the variation of the temperature and velocity profiles and the Nusselt number. The channel geometry and the corresponding coordinate system are shown in Fig. 2. Here, the total flow rate is constant and equal to 10^{-3} l/s. As the external electric field is increased, the pressure gradient is decreased accordingly in order to keep the flow rate constant. The electrical resistivity of water is set to $\sigma = 10^4\ \Omega$m. For the glass/deionized water interface, the electroosmotic mobility $\mu_{eo} = 8\ \mu$m cm/Vs is chosen [33]. The wall heat flux in microchannels, however, can vary over several orders of magnitude. In the present study, the results are presented for three values of wall heat flux, i.e., 1, 10 and 100 W/cm^2.

Fig. 3 shows the velocity and normalized temperature $\theta = (T - T_m)/(q''D/k)$ profiles across the channel for different external electrical fields, E_x. Note that the velocity field and the normalized temperature distributions corresponding to $E_x = 0$ are the same as the conventional pressure driven flow.

As it is observed in Fig. 3a, all velocity profiles intersect with each other at a common point. This point, in fact, is independent of the channel, flow and fluid properties and is the same for all velocity distributions of combined pressure-electroosmotically driven flows described by Eq. (3). If, in Eq. (3), the velocity is set equal to the average velocity, the position of this point is computed as $u = U$ and $Y = \pm 1/\sqrt{12}$. Also, in Fig. 3b, it is observed that as the external electrical field is increased, the difference between the centerline temperature and the wall temperature decreases and consequently the difference between the wall temperature and the bulk mean temperature $T_w - T_m$ declines. As a result, the convective heat transfer coefficient is expected to increase.

In Fig. 4, the normalized temperature θ and the velocity profile are plotted as functions of channel height for different values of wall heat fluxes and external electrical fields. The wall heat flux varies between 1 and 100 W/cm^2 which are typical wall heat fluxes in electronic devices. In Fig. 4b, the electrical field E_x is chosen so that the velocity at the center of the channel becomes zero and no reverse flow occurs in the channel.

In Fig. 4a, it is observed that for low external electrical fields the temperature profile is not sensitive to wall heat flux and is identically the same for all values of the wall heat flux. This is mainly because the velocity profile, in this case, is similar to the conventional parabolic profile of the pressure driven flow. Also, the volumetric heat generation is still negligible. However, as the external electrical field is increased, the temperature field becomes sensitive to the wall heat flux especially in the core of the channel (Fig. 4b). It is observed that as q'' is increased, the difference between the wall temperature and the temperature of the channel core is increased as well, which results in a decrease in the heat transfer coefficient. This will be elaborated below.

In Fig. 5, the normalized temperature θ and the velocity distributions are plotted across the channel for different

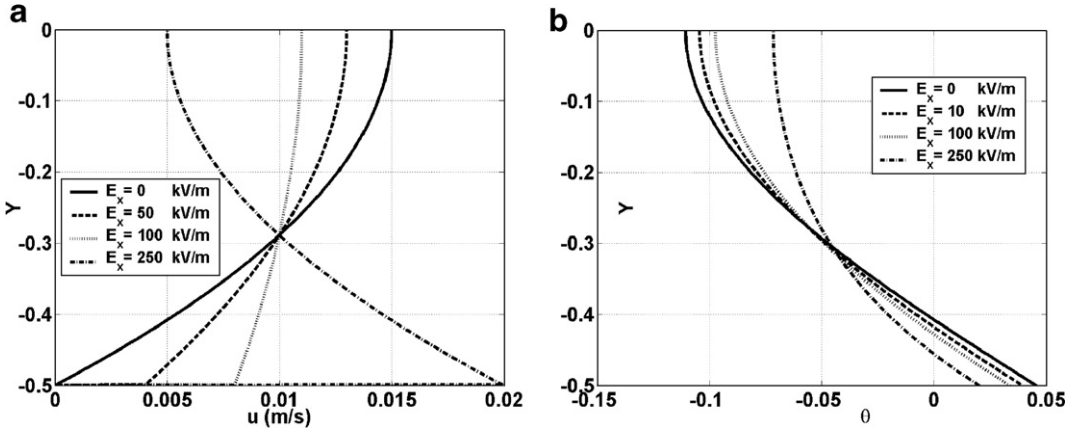

Fig. 3. (a) Velocity field and (b) Normalized temperature distribution for various external electrical fields.

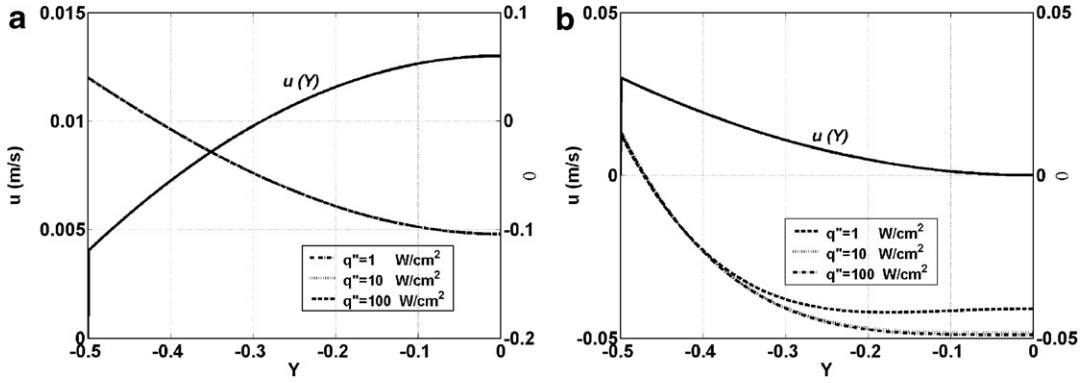

Fig. 4. Normalized temperature and velocity distribution for various wall heat fluxes, (a) $E_x = 50$ kV/m, (b) $E_x = 375$ kV/m.

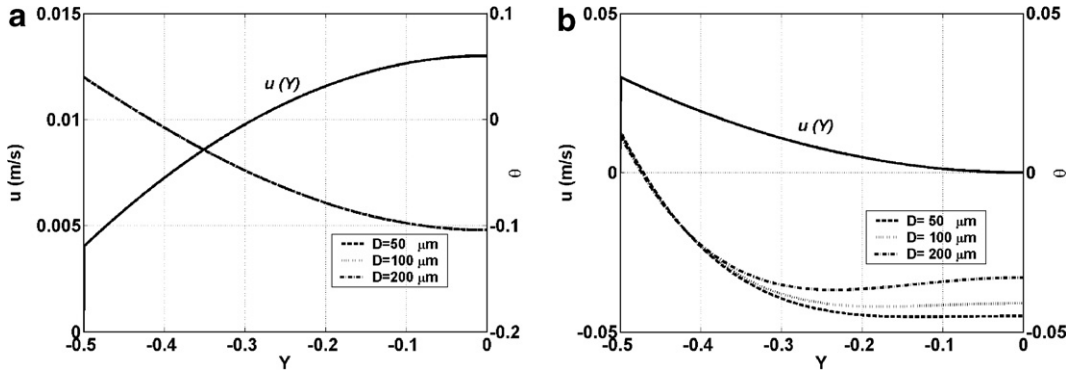

Fig. 5. Normalized temperature and velocity distribution for various channel heights, (a) $E_x = 50$ kV/m, (b) $E_x = 375$ kV/m.

values of the external electrical fields and channel heights for a wall heat flux of $q'' = 10$ W/cm^2. Recall that the velocity distribution, Eq. (3), was obtained with the assumption of high channel height to Debye length ratios, $\Gamma > 50$. Therefore, the minimum channel height is chosen to be 50 μm in the present study.

In Fig. 5a, the temperature profiles show that for low values of E_x, where the flow is still similar to a pressure driven flow and volumetric heat generation is insignificant, the effect of channel height on the temperature profile is negligible. However, as the external electrical field is increased (Fig. 5b) the temperature profile becomes responsive to the channel height particularly in the core of the channel. It is obvious that as the channel height D is increased, the difference between the core temperature and the wall temperature is decreased which results in an increase in the convective heat transfer coefficient. This effect will be discussed later.

As the velocity field and the temperature distribution across the channels vary, it is expected that the corresponding Nusselt numbers vary as well. It was seen in Fig. 3a that as the external electrical field is increased, the velocity near the channel wall increases. This phenomenon can increase the rate of convection heat transfer. On the other hand, an increase in the external electrical field increases the magnitude of the Joule heating effect, which in turn decreases the heat transfer rate. Therefore, there must be a maximum heat transfer rate for each configuration. Fig. 6 shows the variation of Nusselt number in a fully developed regime versus the magnitude of the external electrical field for various q'' and D. In Fig. 6a, the channel height $D = 100$ μm is constant and the wall heat flux effect is investigated while in Fig. 6b the wall heat flux $q'' = 1$ W/cm^2 is constant with varying channel height.

As stated before, the change in velocity profile, and consequently the temperature profile, will affect the heat transfer coefficient. As shown in Fig. 6, in a constant flow rate, a Nusselt number up to approximately five times that of the pressure driven flow can be achieved. This high value of the Nusselt number is associated to the decreasing normalized wall temperature due to stagnant (and sometimes reversing) flow region in the core of the channel. Further examination of Fig. 6 reveals that the maximum Nusselt number and its associated external electrical field depend on the wall heat flux and the channel height. As q'' is increased, with channel height fixed, the maximum Nusselt number decreases, while the corresponding E_x increases. However, it is that the dependency of the Nusselt number on the wall heat flux diminishes with increasing q''. Also, as illustrated in Fig. 6b, with q'' fixed, an increase in channel height increases the Nusselt number.

The electroosmotic mobility μ_{eo} can also change the heat transfer properties since it directly affects the velocity profile. Also it should be noted that in practice, as the elec-

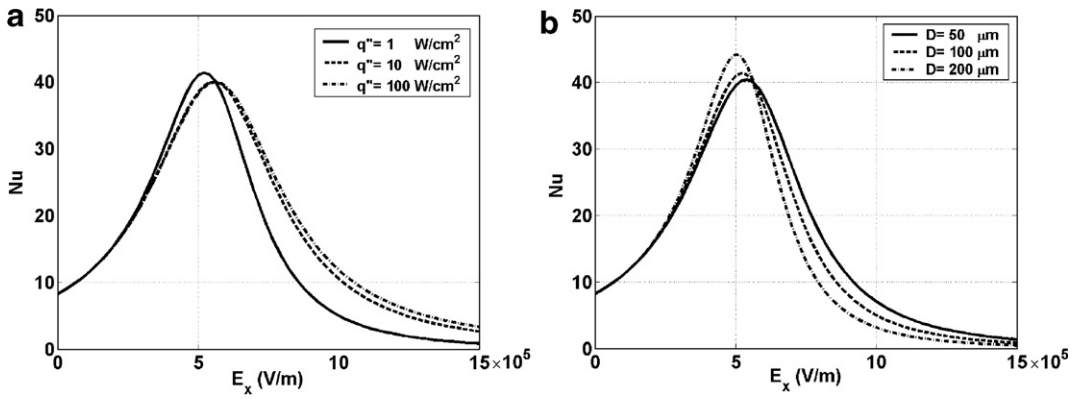

Fig. 6. Nusselt number as a function of external electrical field, (a) $D = 100$ μm, (b) $q'' = 1$ W/cm^2.

troosmotic mobility decreases, or equivalently when the solution concentration increases, the electrical resistivity decreases. In Fig. 7a, the variation of Nusselt number versus the external electrical field is plotted for three electroosmotic mobilities of 6, 8, 10 μm cm/Vs with electrical resistivities of 1, 10 and 100 k Ωm, respectively. The channel height and the wall heat flux are considered to be 100 μm and 10 W/cm^2, respectively. As it is observed, the peak value of the Nusselt number increases but the associated E_x decreases as the electroosmotic mobility is increased. These variations can be better observed in Fig. 7b, where the Nusselt number is plotted as a function of both the external electrical field and the electroosmotic mobility. Again the electrical resistivity is increased with increasing electroosmotic mobility. Interestingly, the dependence of the Nusselt number on the electroosmotic mobility diminishes as μ_{eo} is decreased.

However, heat transfer characteristics do not always exhibit such smooth behaviors. When the volumetric heat generation is sufficiently high to cause the temperature in the stagnant core of the channel to exceed the wall temperature, and the resulting bulk mean temperature to exceed the wall temperature, then the Nusselt number can become negative. Should the electroosmotic mobility, and correspondingly the electrical resistivity, increased beyond a critical value, the Nusselt number may exhibit singularities. In Fig. 8a, this is shown for $\mu_{eo} = 12$ μm cm/Vs, $\sigma = 1 \times 10^6$ Ωm, $q'' = 1$ W/cm^2 and $D = 100$ μm. In general, this critical value is a function of the wall heat flux and channel height and generally occurs for smaller values of both parameters.

In the first singularity point, the temperature in the core of the channel increases so much due to the Joule heating effect that the bulk mean temperature of the flow exceeds the wall temperature and the Nusselt number becomes negative. In the second point, although the core temperature increases even more, but the reverse flow velocity in the core of the channel also increases, so that the bulk mean temperature again falls below the wall temperature and the Nusselt number becomes positive. In Fig. 8b, the normalized temperature profiles for four E_x values before and after singularity points, depicted in Fig. 8a, are shown. Considering the definition of the normalized temperature, it is evident that $\theta_m = 0$. Therefore, the sign of the normalized wall temperature determines the sign of the Nusselt number. A close examination of Fig. 8b reveals that the wall normalized temperatures are 0.0038, −0.0038, −0.0019 and 0.0038 for points 1–4 in Fig. 8a, respectively.

This can also be easily seen in Fig. 9 where the wall normalized temperature θ_w is plotted versus the external

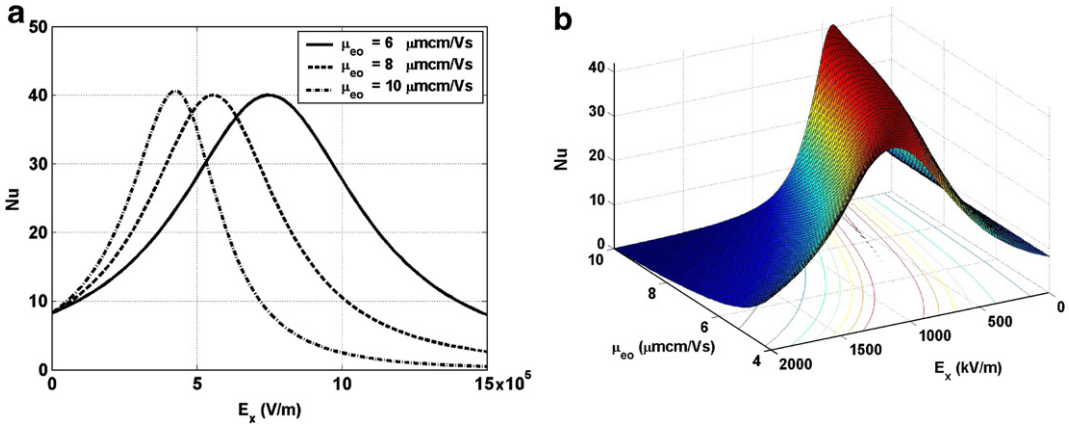

Fig. 7. Nusselt number as a function of external electrical field for various electroosmotic mobilities.

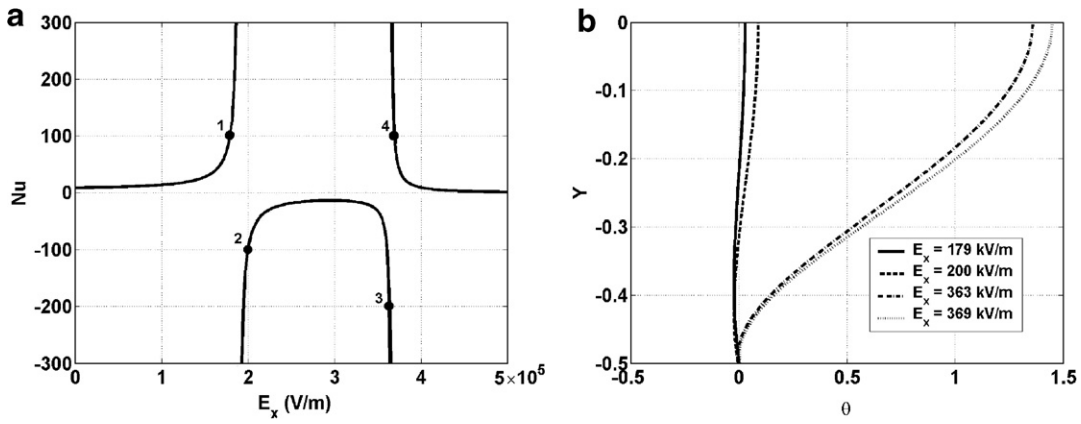

Fig. 8. (a) Nusselt number and (b) θ across the channel as functions of external electrical field for high electroosmotic mobilities.

electrical field for various electroosmotic mobilities of 6, 8, 10 and 12 μm cm/Vs with electrical resistivities of 1, 10, 100 and 1000 k Ωm, respectively. In this figure, the channel height and the wall heat flux are $D = 100$ μm and $q'' = 1$ W/cm^2, respectively. As stated before, considering the definition of the normalized temperature, the sign of the wall normalized temperature determines the sign of the Nusselt number. It is observed from Fig. 9 that when the electroosmotic mobility is increased beyond a critical value, the wall normalized temperature changes sign twice as the external electrical field is increased. It is seen that for the case of $\mu_{eo} = 12$ μm cm/Vs the wall normalized temperature becomes zero at $E_x = 189$ kV/m and $E_x = 365$ kV/m which are clearly the points of singularity in Fig. 8a. Between these values of the external electrical field, where the wall normalized temperature is negative, the Nusselt number is also negative.

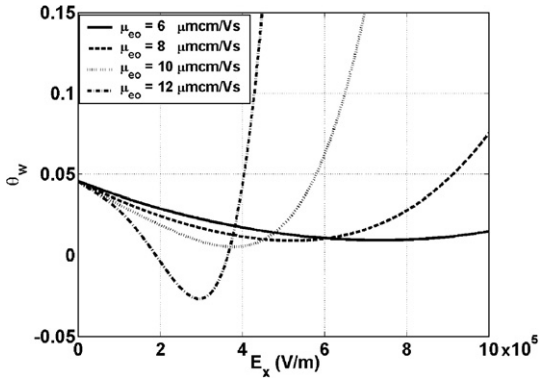

Fig. 9. Wall normalized temperature vs. external electrical field for different electroosmotic mobilities.

In order to study the effect of the flow rate on the heat transfer characteristics of the system, in the proceeding results, the pressure gradient is considered to be constant and then as the external electrical field is increased the mean velocity, and in turn, the flow rate is increased. Fig. 10 shows the velocity and normalized temperature profiles across the channel for different external electrical fields, E_x. As it is observed in Fig. 10a, since the flow rate is not fixed, an increase in external electrical field directly increases the mean velocity as well as the velocity at the center of the channel. Also, in Fig. 10b, it is observed that as the external electrical field is increased, the difference between the centerline temperature and the wall temperature decreases and consequently the difference between the wall temperature and the bulk mean temperature $T_w - T_m$ declines. As a result, the convective heat transfer coefficient is expected to increase. This trend, however,

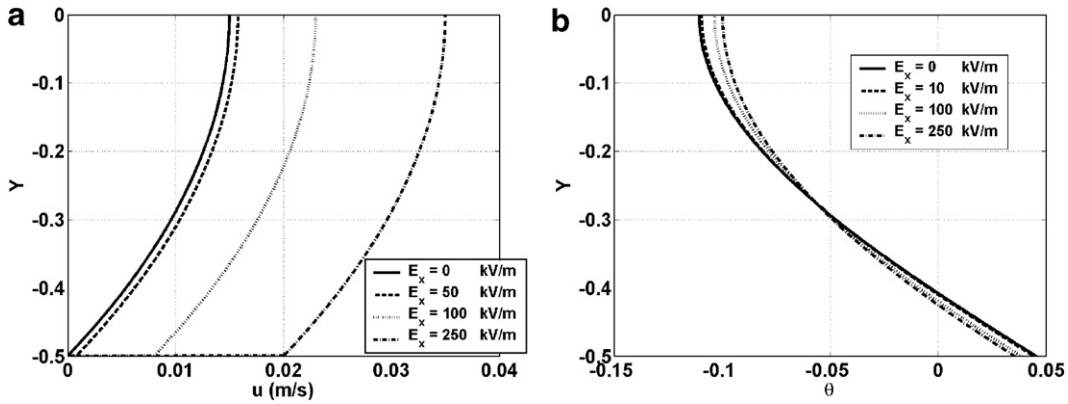

Fig. 10. (a) Velocity field and (b) Normalized temperature distribution for various external electrical fields with constant pressure gradient.

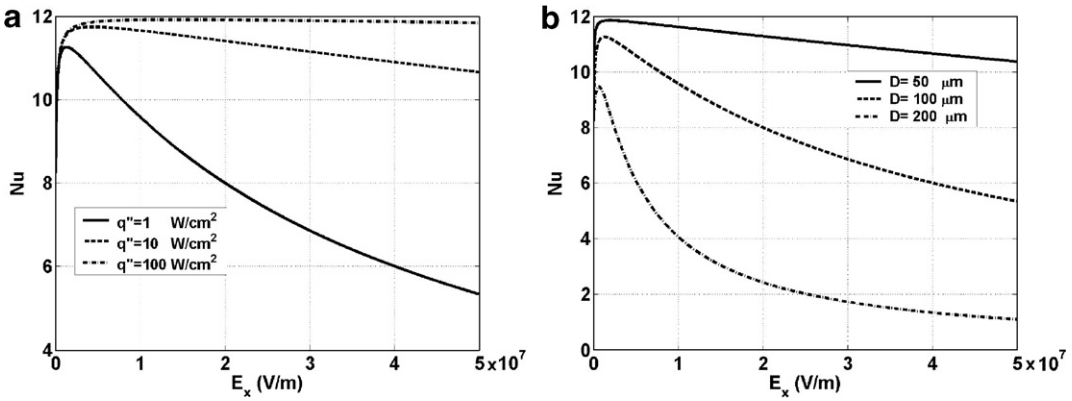

Fig. 11. Nusselt number as a function of external electrical field, (a) $D = 100$ μm, (b) $q'' = 1$ W/cm^2 with constant pressure gradient.

does continue up to a point where excessive volumetric heat generation due to increased external electrical field overcomes the increase in flow rate. This dependency is observed clearly in Fig. 11.

In Fig. 11 the flow rate is free to change and considering the range of external electrical field applied, the mean velocity varies from 0.01 m/s to 4 m/s. If there were no volumetric heat generation, as the external electrical field is increased, the velocity profile would tend to become a slug-like flow and the corresponding Nusselt number asymptotically reaches 12. However due to volumetric heat generation, this theoretical value is not reached and the Nusselt number decreases before reaching this theoretical value. This behavior is shown in Fig. 11. From this figure it is also apparent that the Nusselt number depends on the wall heat flux and the channel height. As q'' is increased, with channel height fixed, the maximum Nusselt number increases. Also, as illustrated in Fig. 11b, with q'' fixed, an increase in channel height decreases the Nusselt number.

It should be noted that when the pressure gradient is constant the Nusselt number does not exhibit any singularity. This is mainly because the velocity of the core of the flow does not vanish, unlike the case of prescribed flow rate.

4. Conclusion

Hydrodynamically and thermally fully-developed flow of combined pressure-electroosmotically driven flow in planar microchannels was investigated analytically for a constant wall heat flux boundary condition. Also, the maximum achievable Nusselt number for a range of problem parameters has been investigated. It is shown that the thermally fully-developed temperature distribution and the corresponding Nusselt number are identified by four parameters: the channel height, the imposed wall heat flux, the electroosmotic mobility and the external electrical field. It was also revealed that for a prescribed flow rate the Nusselt number computed for a combined pressure-electroosmotically driven flow can reach up to approximately five times that of the pressure driven flow. It was also shown that the maximum Nusselt number increases by decreasing the wall heat flux, increasing the channel height or increasing the electroosmotic mobility. For a prescribed pressure gradient it was shown that the maximum Nusselt number increases by decreasing the channel height and by increasing the wall heat flux. In the case of a prescribed pressure gradient the Nusselt number increases solely due to an increase in the near wall velocity. In the case of a prescribed flow rate, however, an increase in the near wall velocity decreases the velocity in the core region of the channel which results in much higher Nusselt numbers. Also, it was demonstrated that under certain circumstances, the Nusselt number may become negative and exhibit singularities as the external electrical field varies. This phenomenon occurs when the Joule heating effect (volumetric heat generation) is high enough so that the temperature in the stagnant or slow-moving core of the channel and the resulting bulk mean temperature exceed the wall temperature.

References

[1] D.J. Laser, J.G. Santiago, A review of micropumps, J. Micromech. Microeng. 14 (2004) R35–R64.
[2] P.K. Dasgupta, L. Shaorong, Electroosmosis: A reliable fluid propulsion system for flow injection analysis, Anal. Chem. 66 (1994) 1792–1798.
[3] S. Arulanandam, D. Li, Liquid transport in rectangular microchannels by electroosmotic pumping, J. Colloids Surf. 161 (2000) 29–102.
[4] C.H. Chen, J.G. Santiago, A planar electroosmotic micropump, J. MEMS 11 (2002) 672–683.
[5] F.F. Reuss, Charge-induced flow, Proceedings of the Imperial Society of Naturalists of Moscow 3 (1809) 327–344.
[6] R.J. Hunter, Zeta Potential in Colloidal Science: Principles and Applications, Academic, London, 1981, pp. 1–58.
[7] G.M. Mala, D. Li, C. Werner, H.J. Jacobasch, Y.B. Ning, Flow characteristics of water through a microchannel between two parallel plates with electrokinetic effects, Int. J. Heat Fluid Flow 18 (1997) 489–496.
[8] O. Söderman, B. Jönsson, Electro-osmosis, velocity profiles in different geometries with both temporal and spatial resolution, J. Chem. Phys. 105 (1996) 10300.
[9] J.G. Santiago, Electroosmotic flows in microchannels with finite inertial and pressure forces, Anal. Chem. 73 (2001) 2353–2365.
[10] D. Burgreen, F.R. Nakache, Electrokinetic flow in ultra fine capillary slits, J. Phys. Chem. 68 (1964) 1084–1091.

[11] C.L. Rice, R. Whitehead, Electrokinetic flow in a narrow cylindrical capillary, J. Phys. Chem. 69 (1965) 4017–4024.
[12] S. Levine, J.R. Marriott, G. Neale, N. Epstein, Theory of electrokinetic flow in fine cylindrical capillaries at high zeta-potentials, J. Colloid Interf. Sci. 52 (1974) 136–149.
[13] C. Yang, D. Li, J.H. Masliyah, Modeling liquid flow forced convection in rectangular microchannels with electrokinetic effects, Int. J. Heat Mass Transfer 41 (1998) 4229–4249.
[14] C. Yang, C.B. Ng, V. Chan, Transient analysis of electroosmotic flow in a slit microchannel, J. Colloid Interf. Sci. 248 (2002) 524–527.
[15] T.L. Sounart, J.C. Baygents, Electrically-driven fluid motion in channels with streamwise gradients of the electrical conductivity, Colloids Surf. A 195 (2001) 59–75.
[16] X.Y. Chen, K.C. Toh, J.C. Chai, C. Yang, Developing pressure-driven liquid flow in microchannels under the electrokinetic effect, Int. J. Eng. Sci. 42 (2004) 609–622.
[17] J.P. Gleeson, Electroosmotic flows with random zeta potential, J. Colloid Interf. Sci. 249 (2002) 217–226.
[18] A.E. Herr, J.I. Molho, J.G. Santiago, M.G. Mungal, T.W. Kenny, M.G. Garguilo, Electroosmotic capillary flow with nonuniform zeta potential, Anal. Chem. 72 (2000) 1053–1057.
[19] T. Tsuda, M. Ikedo, Observation of flow profiles in electroosmosis in a rectangular capillary, J. Chromatogr. 632 (1993) 201–207.
[20] P.H. Paul, M.G. Garguilo, D.J. Rakestraw, Imaging of pressure- and electrokinetically driven flows through open capillaries, Anal. Chem. 70 (1998) 2459–2467.
[21] E.B. Cummings, PIV measurement of electro-osmotic and pressure-driven flow components in microfluidic systems, J. MEMS 1 (1999) 377–384.
[22] D. Sinton, D. Li, Electroosmotic velocity profiles in microchannels, Colloids Surf. A 222 (2003) 273–283.
[23] W.R. Lempert, K. Magee, P. Ronney, K.R. Gee, R.P. Haugland, Flow tagging velocimetry in incompressible flow using photo-activated nonintrusive tracking of molecular motion (PHANTOMM), Exp. Fluids 18 (1995) 249–257.
[24] T.E. Valko, H. Siren, M. Riekkola, Characteristics of electro-osmotic flow in capillary electropheresis in water and in organic solvents without added ionic species, J. Microcolumn Separa. 11 (1999) 199–208.
[25] W.M. Kays, M.E. Crawford, Convective Heat and Mass Transfer, McGraw Hill, 1993.
[26] D. Li, Electro-viscous effects on pressure-driven liquid flow in microchannels, J. Colloids Surf. A 195 (2001) 35–57.
[27] C.Y. Soong, S.H. Wang, Theoretical analysis of electrokinetic flow and heat transfer in a microchannel under asymmetric boundary conditions, J. Colloid Interf. Sci. 265 (2003) 202–213.
[28] D. Maynes, B.W. Webb, Fully developed electro-osmotic heat transfer in microchannels, Int. J. Heat Mass Transfer 46 (2003) 1359–1369.
[29] D. Maynes, B.W. Webb, The effect of viscous dissipation in thermally fully-developed electro-osmotic heat transfer in microchannels, Int. J. Heat Mass Transfer 47 (2004) 987–999.
[30] D. Maynes, B.W. Webb, Fully-developed thermal transport in combined pressure and electro-osmotically driven flow in microchannels, ASME J. Heat Transfer 125 (2003) 889–895.
[31] R.F. Probstein, Physicochemical Hydrodynamics, second ed., Wiley, New York, 1994.
[32] N.T. Nguyen, S.T. Wereley, Fundamentals and Applications of Microfluidics, Artech House, 2002.
[33] M.H. Oddy, J.G. Santiago, A method for determining electrophoretic and electroosmotic mobilities using AC and DC electric field particle displacements, J. Colloid Interf. Sci. 269 (2004) 192–204.